

Attenuation of ice-sheet reverberations in teleseismic P-wave receiver functions

Dale Harpley

Velseis Pty Ltd & University of Qld
daleh@velseis.com

Steve Hearn

Velseis Pty Ltd & University of Qld
steveh@velseis.com

Shaun Strong

Velseis Pty Ltd
sstrong@velseis.com

SUMMARY

Teleseismic P -wave receiver functions (PRFs) in ice-covered regions are contaminated by reverberations within the ice-sheet. The crustal conversion events which are commonly used for identifying lithospheric structure are concealed by these ice reverberations.

The problematic ice-phase reverberations can, however, be exploited. We describe a practical process, incorporating a simple generalised linear inversion (GLI) stage, which yields an ice-sheet model.

The derived ice model can then be used to design a Wiener filter aimed at attenuating ice phases, and revealing crustal phases in the PRF. Although it is theoretically approximate, the Wiener approach appears robust. Synthetic trialling, using realistic models, is essential for understanding the limitations of the algorithm.

The full process has been applied at ice-covered stations in Antarctica and Greenland. In each case, we have derived robust models for the ice, and have successfully extracted crustal P_s phases from the contaminated receiver functions.

Key words: Receiver function, ice-sheet reverberations, Wiener filtering, predictive deconvolution.

INTRODUCTION

The receiver function technique is commonly applied to teleseismic P -waves, to estimate crustal structure below a recording station (Langston, 1979). For the P arrival, the vertical component is deconvolved from the horizontal (i.e. radial or transverse components) by spectral division. The teleseismic source signature is also assumed to be removed by the deconvolution, revealing crustal information below the receiver. The events on P -wave receiver functions (PRFs) relate to the lag-time (time with respect to the initial P arrival) of converted and multiple phases. Figure 1 illustrates our notation for example phases P_s and $Ppps$, for a simple layered crust. The ideal radial P -wave receiver function corresponding to the simple model in Figure 1 is shown in Figure 2a.

The ice-bedrock boundary in polar regions has a large acoustic-impedance contrast which introduces reverberations on teleseismic seismograms, and hence on PRFs. As shown in Figure 2b, the ice-phase conversions and multiples produce very high-amplitudes at short lag-times in the PRF. These ice reverberations make confident identification of the crustal phases impossible.

Our primary purpose in this paper is to demonstrate a Wiener-filtering approach to attenuate the interference of the ice-phases. As a preliminary, we also outline how the problematic ice phases can be used to determine the ice-sheet properties. The ice model is needed to design the Wiener filter.

Methods of ice-reverberation suppression have been explored previously. For example, Chai et al., (2017) deconvolved downward-continued seismic wave vectors to create PRFs which minimise the ice-layer reverberations. Ramirez et al. (2016) analyse the Moho S_p conversion in S -wave receiver functions.

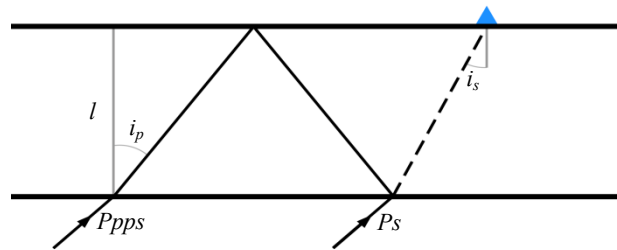


Figure 1. Diagram of ray-paths of phases P_s and $Ppps$ to a receiver above a single layer. Solid and dashed lines denote P - and S -wave segments. Upper and lower case letters denote wave type in the half-space and layer respectively.

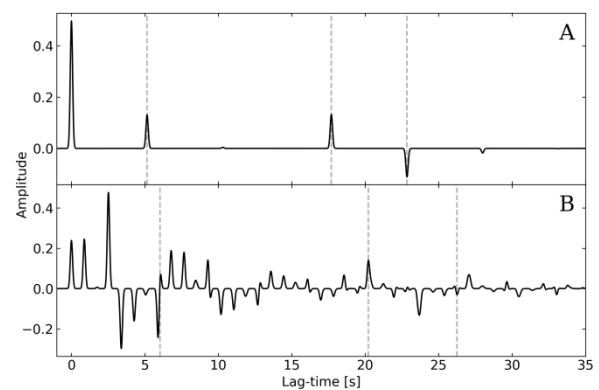


Figure 2. Simple radial PRF examples, with dashed lines for crustal phases P_s , $Ppps$, and Pps . a) Average crust above mantle halfspace; and b) ice-sheet above identical crustal model and halfspace.

This study illustrates an alternative approach to predicting ice-sheet properties, bedrock shear-wave velocity, and crustal thicknesses in ice-covered regions, such as Antarctica and Greenland. Ice-sheet parameters are derived via a simple constrained inversion of PRF phase times. The derived ice model is then used to design a Wiener filter which attenuates ice reverberations, allowing improved interpretation of the crustal P_s phase.

ICE-SHEET MODELLING

The measured lag-times of the ice-phases provide an opportunity to use a simple generalised linear inversion (GLI) to predict ice-layer parameters (thickness, P - and S -wave velocities). The measured ice-phase lag-times can be matched to a synthetic ice-layer PRF created with the Thomson-Haskell matrix formalism (Haskell, 1953, 1962). Note that there is intrinsic non-uniqueness between ice thickness and ice velocity. Non-uniqueness is limited by using constraints on the body-wave velocities, based on estimation of the P -wave incident angle (i_p , derived from hodogram analysis) and the v_p/v_s ratio in the ice.

Identification of ice phases in PRF

Peaks in the PRF relate to the lag-time between the P arrival and the respective conversion, or multiple. These lags can be calculated using layer equivalent-time formulae (e.g. Hearn, 1981).

$$t_p = \frac{l \cos i_p}{v_p} ; \quad t_s = \frac{l \cos i_s}{v_s} \quad (1)$$

where l , i , and v denote layer properties: thickness, incident angle, and velocity. For example, Equation 2 shows the first two phase lags (P_s and P_{pps}) for a single layer PRF.

$$\tau_{P_s} = t_s - t_p ; \quad \tau_{P_{pps}} = 2t_p + t_s - t_p = t_s + t_p \quad (2)$$

Note that all lags will contain a subtraction of the P -wave equivalent layer time so that the main P phase event is $\tau=0s$.

Estimation of ice-sheet v_p/v_s ratio

Referring to Equation 2, if two suitable lags (τ) can be identified in the real-data PRFs then the equivalent times in the ice, t_p and t_s , can be derived. As an example, at a site in Antarctica (Concordia) at least four ice-phases are able to be confidently picked at Concordia giving an overdetermined system. A simple inversion with singular value decomposition (SVD) can then be used to find t_p and t_s .

Once the equivalent times are estimated, we can estimate the velocity ratio γ and S -wave incidence (i_s), using an iterative approach based on Equation 3.

$$\gamma = \frac{v_p}{v_s} = \frac{t_s \cos i_p}{t_p \cos i_s} \quad (3)$$

Generalised linear inversion

The GLI algorithm (Wiggins, 1972) is commonly applied in geophysics to solve an overdetermined system in the form Jacobian $\mathbf{J}\mathbf{x}=\mathbf{y}$. Where \mathbf{x} is the change in model parameters, \mathbf{y} is the change in observations, and \mathbf{J} is the sensitivity matrix.

For our problem we need to create an ice-sheet model where the PRF lag-times match measured values. The unknown ice parameters that control these lags are l , v_p and v_s (Equations 1, 2) (i_p is known and ice density is assumed to be 0.917g/cc). The starting model is perturbed for each parameter and the Jacobian (\mathbf{J}) is built with central finite-differences. The \mathbf{y} vector contains differential lags of ice-phases in the PRF (e.g. $\delta\tau_{P_s}$, $\delta\tau_{P_{pps}}$, $\delta\tau_{P_{sss}}$). The \mathbf{x} vector (containing δl , δv_p , δv_s) is solved using SVD, and the model is updated. v_s and i_s are

constrained by v_p/v_s and i_p computed for the given station. The best fit solution is picked by the shortest number of SVD iterations and minimum error of \mathbf{y} after solving over different initial models varying l and v_p .

Estimation of bedrock parameters

For the following Wiener filter design phase, the ice-model PRFs required a known halfspace basement. Based on findings by Julià (2007) the P_s phase amplitude in the receiver function is predominantly controlled by the v_s contrast at that boundary. We have used the ice P_s amplitude to estimate bedrock v_s at all stations. (We will use the term bedrock to refer to the rock layer directly under the ice.) Bedrock density and v_p are then inferred using empirical relations between wave velocities and density (Equation 11 in Brocher, 2005).

Derived ice-sheet models

We have applied this process to two stations in Antarctica (Concordia, CCD; Marie Byrd Land, BYRD), and one in Greenland (Eemian, NEEM). The derived ice models are summarised in Table 1 (Page 5).

WIENER FILTERING: SYNTHETIC TRIALS

The previous section outlined the process of estimating ice-sheet parameters based on PRF observations. The derived ice model provides the starting point for the Wiener attenuation. First we illustrate the concepts using synthetic models. Figure 3 shows v_p and v_s for representative models. Average crustal density has been assumed to be 2.81g/cc. The multilayered crustal model has the same average crustal parameters. With increasing complexity of the crust, the amplitudes of crustal-phases in the PRF generally reduce. Use of a more realistic model provides better insight into the behaviour of Wiener filters and their application to real data.

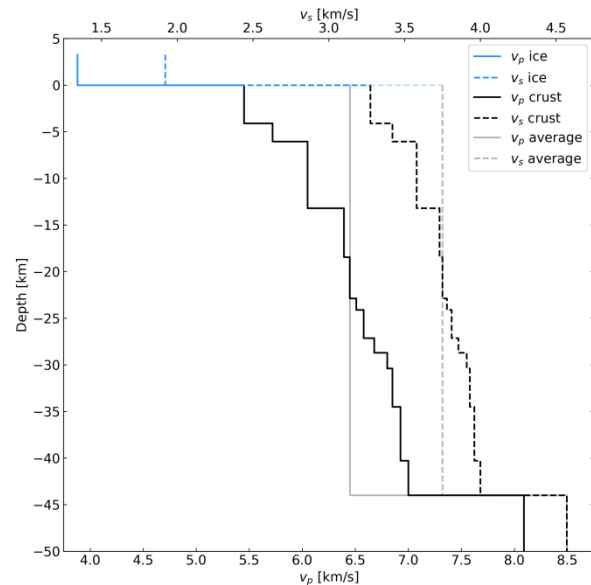


Figure 3. Synthetic ice and crust models used for receiver function modelling. Depth is with respect to the base of the ice-sheet. Average CCD ice model (blue) parameters listed in Table 1. Average crustal body-wave velocities: $v_p=6.45\text{km/s}$ and $v_s=3.75\text{km/s}$ (grey).

Wiener filtering (signature deconvolution)

Here we consider standard or deterministic Wiener filtering, sometimes called signature deconvolution (e.g. Robinson and Treitel, 2000). The hypothesis is that a Wiener spiking filter designed on a pure-ice PRF should act to attenuate ice phases in an ice-crust PRF. As illustrated below this is an approximation (Figure 5).

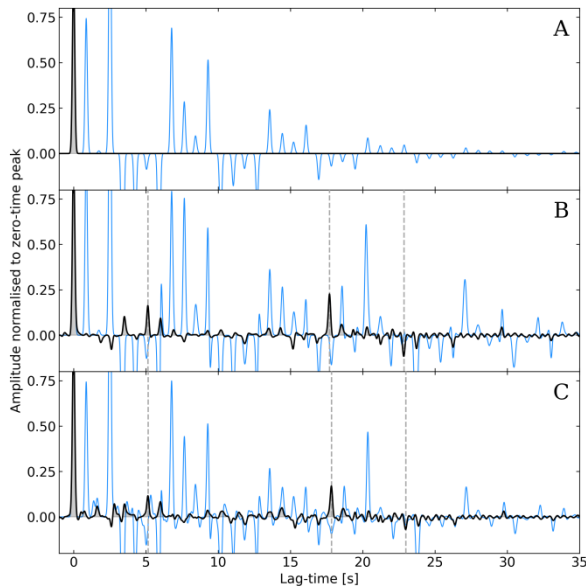


Figure 4. Synthetic PRFs (blue) and filtered results (black). Dashed lines show ice-removed lag-times of Moho phases: *Ps*, *Ppps*, and *Ppss*. a) Average CCD ice model PRF (blue), filtered into the desired zero-time peak (black); b) Single layered average crust below ice; and c) Multilayered crust below ice.

Figure 4a illustrates that a Wiener filter can be designed to compress the ice-layer PRF into a peak at $\tau=0$ s. (Here we have used a non-causal frequency-domain approach.) When applied to the ice-crust PRFs (Figures 4b-c), the ice-phases have been significantly attenuated, although there are artefacts. Note that the Wiener filter shifts crustal events in time, effectively simulating recording under the ice-layer.

Because the method is an approximation, the crustal *Ps* phase (~ 5 s) only appears slightly greater in amplitude than some of the spurious peaks which remain after filtering. The *Ppps* crustal phase (~ 18 s) is less affected by artefacts, being a stronger event in noise-free PRFs to begin with.

Convolutional model assessment

For the previous approach to perform perfectly, we would require that the PRF of a multilayered earth is the convolution of individual layer PRFs. The receiver function does not strictly satisfy this assumption, resulting in filter artefacts. Figure 5 gives an example of the imperfection in the convolutional assumption. The ice-crust PRF (blue) is very similar, but not identical, to the individual PRFs convolved (black). This limitation has been noted previously by Cho (2011) who investigated a different deconvolution process. The accuracy of the approximation varies from model to model and with other processing parameters.

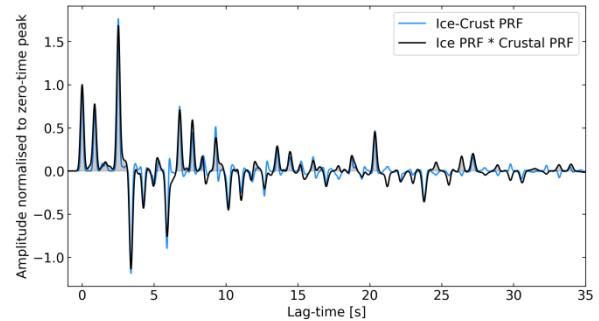


Figure 5. Comparison between the convolution of an ice PRF with a single layer crust PRF (black) and the true ice-crust PRF (blue).

More detailed intuitive explanations can be given for the acknowledged limitations in our filtering process. In Figure 5, each of the single-layer models would include surface effects, while the multilayered model only allows for the true surface. Also, the Wiener filter is designed for a *P*-wave incident on the base of ice, and this would not properly compress incident *S* phases. Given these imperfections, we have been surprised at the general effectiveness of the approach.

REAL-DATA APPLICATION

Wiener filtering

For each station we have applied the full Wiener-filter process to PRFs from individual earthquakes, as well as for the stacked PRF. In general the latter is preferred, because the stacking process reduces noise somewhat. Figure 6 shows the result of Wiener filtering of stacked PRFs from stations CCD, BYRD, and NEEM.

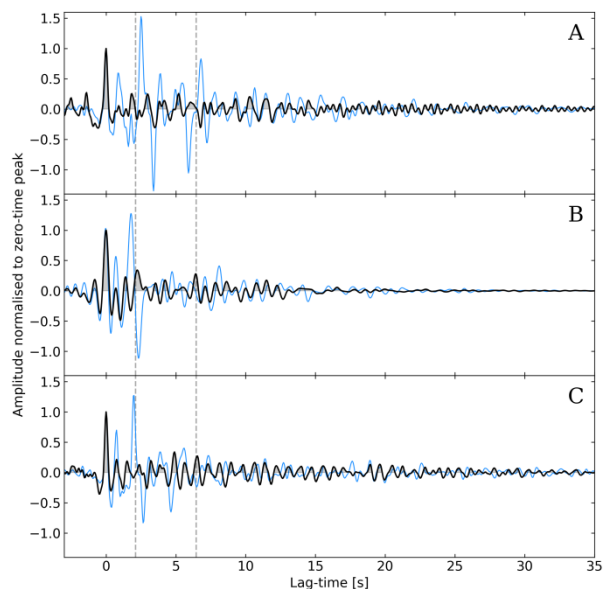


Figure 6. Wiener filter designed on average ice model applied to real-data stacked PRFs at a) CCD, b) BYRD, and c) NEEM. Stacked PRFs (blue), filtered PRFs (black), and dashed lines indicate the expected time range for the Moho *Ps* for an average crustal model between ~ 20 - 55 km.

Although the final results are noisy, the successful attenuation of the original ice reverberations (blue) is a very positive result. Interpretation of Figure 6 is difficult because the filtered traces

are noisy. It should, however, be noted that PRF crustal phases are often quite difficult to identify even for stations without ice. Our interpretation of Figure 6 is given in a later section.

Predictive deconvolution

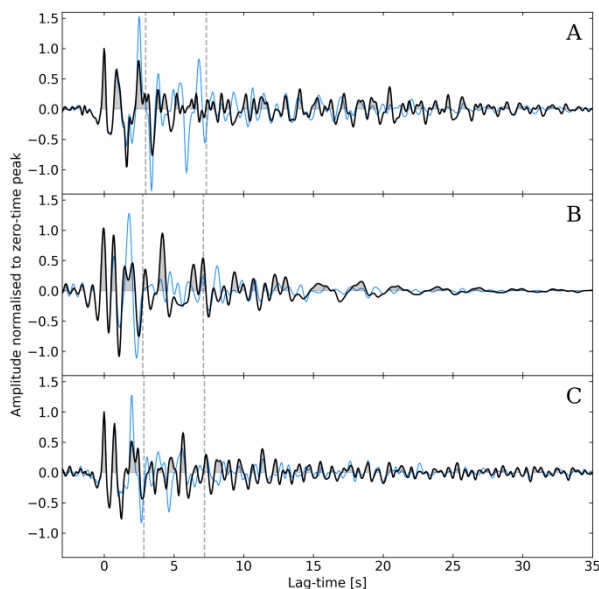


Figure 7. Predictive error filter designed on averaged ice model applied to real-data stacked PRFs at a) CCD, b) BYRD, and c) NEEM. Stacked PRFs (blue), filtered PRFs (black), and dashed lines indicate the expected time range for the Moho P_s (including ice-layer) for an average crustal model between ~ 20 – 55 km.

Because predictive deconvolution is a standard in seismic processing, it is interesting to consider it here. In the context of reflection seismology, the basic assumptions of predictive deconvolution are random reflectivity, minimum-phase wavelet, and no noise. Transferring the concept to our problem, arguably none of these assumptions is satisfied. Hence our tests are purely empirical. Synthetic trials illustrate that, in many cases, predictive deconvolution does significantly attenuate ice reverberations in the PRF, although the ice-bedrock P_s conversion is either unaffected or amplified. The predictive operator can overcompensate when removing ice-phases and introduce new peaks. Overall, performance of predictive deconvolution is very model dependent, and is considered less robust than the standard Wiener filtering approach.

For interest, Figure 7 gives the output of predictive deconvolution at the three ice stations, again applied to stacked PRFs. (The prediction gap is the second zero crossing in the autocorrelation. The prediction filter length is 40s.) It is important to note that predictive deconvolution does not include the time correction provided by the Wiener approach. Hence we expect a known time shift between the two estimates of the crustal P_s phase, equal to the ice-bedrock P_s lag time.

At stations BYRD and NEEM, large peaks are observed (Figures 7b-c) within the expected time window for the Moho P_s . No obvious peak has been observed at CCD (Figure 7a) which could be explained by the thicker ice-sheet, i.e. later lag-times interfering more severely with the Moho P_s .

INTERPRETATION OF FILTERED PRFS

The following describes a potential method of interpretation based on lags from the filtered PRFs. The interpreted lag-times and resulting Moho depth estimates are listed in Table 2.

CCD. A potential P_s Moho conversion has been picked in Figure 6a at ~ 5.2 s. Although the amplitude of this peak is similar to noise, identification is assisted by knowledge of the expected polarity, and expected time range. This peak suggests a thicker than average crust, which is supported by other experiments (e.g. Ramirez et al. 2016).

BYRD. In Figure 6b, the largest positive peak within the expected Moho P_s window is at ~ 2.2 s. This lag is not consistent with the strong peak exhibited in the predictive deconvolution result (Figure 7b) of ~ 4.2 s (including ice-bedrock P_s lag). The predictive deconvolution result is preferred because of the strong peak amplitude. This would correspond to a thin crust as suggested by Chai et al. (2017).

NEEM. Peaks have been observed at ~ 4.9 s (Figure 6c) and ~ 5.65 s (Figure 7c). In this example the expected time shift introduced between the Wiener and predictive filters is ~ 0.75 s. This implies excellent agreement, supporting a true crustal P_s phase. An average crustal thickness is suggested.

Station	Ice P_s [s]	Moho		Depth range [km]
		P_s Wiener [s]	P_s Pred. Decon. [s]	
CCD	0.87	5.2	N/A	43.5 – 45.5
BYRD	0.69	2.2	4.2	18.5 – 30.6
NEEM	0.75	4.9	5.65	40.9 – 42.8

Table 2. Interpretation results of filtered PRFs. Ice P_s refers to the ice-bedrock P_s phase. Moho depth is with reference to the base of the ice-sheet, and range considers incident angles between 20 – 35° at the top of mantle. Predictive deconvolution lags include the ice P_s lag.

CONCLUSIONS

We have demonstrated a Wiener filtering process for attenuating ice reverberations in teleseismic PRFs. This allows more reliable interpretation of crustal phases.

The preliminary stage takes advantage of the ice reverberations to model the ice-sheet. Approximations of the v_p/v_s ratio and the ice-sheet incident angle help to constrain the GLI inversion. Estimates of the bedrock shear velocity have also been inferred. Ice-sheet parameters have been estimated at stations CCD and BYRD in Antarctica, and NEEM in Greenland.

The derived ice model can be used to design a Wiener filter which will, in theory, compress all ice reverberations. Consideration of the convolutional model clarifies why this is an approximate solution. Nevertheless, the approach can give viable results if used with caution.

In pragmatic testing, predictive deconvolution sometimes yields a stronger Moho P_s event. However, it is considered less robust than Wiener filtering. Use of both methods in parallel might provide additional control. Synthetic trials, using models relevant to the real situation, are invaluable for understanding

the performance of the process, and for identifying the most likely real-data phases.

The filtering process has extracted identifiable crustal P_s phases, allowing estimates of crustal thickness at CCD, BYRD and NEEM.

ACKNOWLEDGMENTS

This project originated as an honours thesis at The University of Queensland.

All seismic data were downloaded through the IRIS Wilber 3 system, including the following seismic networks: (1) the G (GEOSCOPE; IPGP and EOST, 1982); (2) the YT (IPY POLENET-Antarctica; Wiens and Nyblade, 2007); and (3) the DK (Danish National Seismic Network, 1980).

REFERENCES

- Bentley, C.R., 1972, Seismic-wave velocities in anisotropic ice: A comparison of measured and calculated values in and around the deep drill hole at Byrd Station, Antarctica: *Journal of Geophysical Research*, 77(23), 4406-4420.
- Brocher, T.M., 2005, Empirical relations between elastic wavespeeds and density in the earth's crust: *Bulletin of the Seismological Society of America*, 95(6), 2081-2092.
- Chai, C., Ammon, C.J., Anandkrishnan, S., Ramirez, C., and Nyblade, A., 2017, Estimating subglacial structure using P-wave receiver functions: *Geophysical Journal International*, 209(2), 1064-1079.
- Cho, T., 2011, Removing reverberation in ice sheets from receiver functions: *Seismological Research Letters*, 82(2), 207-210.
- Haskell, N.A., 1953, The dispersion of surface waves on multilayered media: *Bulletin of the Seismological Society of America*, 43(1), 17-34.
- Haskell, N.A., 1962, Crustal reflection of plane P and SV waves: *Journal of Geophysical Research*, 67(12), 4751-4768.
- Hearn, S., 1981, Applications of teleseismic P phases to structure of the crust and upper mantle in Eastern Queensland, Australia: Ph.D. Thesis, The University of Queensland.
- Institut de Physique du Globe de Paris (IPGP) and Ecole et Observatoire des Sciences de La Terre de Strasbourg (EOST), 1982, GEOSCOPE, French Global Network of broad band seismic stations: IPGP, Université de Paris.
- Julià, J., 2007, Constraining velocity and density contrasts across the crust–mantle boundary with receiver function amplitudes: *Geophysical Journal International*, 171(1), 286-301.
- Langston, C.A., 1979, Structure under Mount Rainer, Washington, inferred from teleseismic body waves: *Journal of Geophysical Research: Solid Earth*, 84(B9), 4749-4762.
- Montagnat, M., Azuma, N., Dahl-Jensen, D., Eichler, J., Fujita, S., Gillet-Chaulet, F., Kipfstuhl, S., Samyn, D., Svensson, A. and Weikusat, I., 2014, Fabric measurement along the NEEM ice core, Greenland, and comparison with GRIP and NGRIP ice cores: *The Cryosphere Discuss*, 8, 307-335.
- Parrenin, F., Barnola, J.M., Beer, J., Blunier, T., Castellano, E., Chappellaz, J., Dreyfus, G., Fischer, H., Fujita, S., Jouzel, J. and Kawamura, K., 2007, The EDC3 chronology for the EPICA Dome C ice core: *Climate of the Past*, 3(3), 485-497.
- Ramirez, C., Nyblade, A., Anandkrishnan, S., Hansen, S., Wiens, D., Shore, P., Aster, R., Huerta, A., and Wilson, T., 2016, Crustal and upper-mantle structure beneath ice-covered regions in Antarctica from S-wave receiver functions and implications for heat flow: *Geophysical Journal International*, 204(3), 1636-1648.
- Robinson, E. and Treitel, S., 2000, *Geophysical Signal Analysis*, Society of Exploration Geophysicists.
- Wiens, D., and Nyblade, A., 2007, IPY POLENET-Antarctica: Investigating links between geodynamics and ice sheets: *International Federation of Digital Seismograph Networks*.
- Wiggins, R.A., 1972, The general linear inverse problem: Implication of surface waves and free oscillations for earth structure: *Reviews of Geophysics*, 10(1), 251-285.

Station I.D.	Station name	Ice core [km]	Ice l [km]	% error	Ice v_p [km/s]	Ice v_s [km/s]	Ice v_p/v_s	Bedrock v_s [km/s]	No. of PRFs
CCD	Concordia, East Antarctica	3.275	3.278	0.09	3.878	1.919	2.022	3.275	15
BYRD	Marie Byrd Land, West Antarctica	2.164	2.138	1.2	3.831	1.79	2.143	2.875	5
NEEM	Eemian, Greenland	2.461	2.475	0.57	3.85	1.829	2.107	3.04	6

Table 1. Ice stations, average inversion results for ice parameters, bedrock v_s estimate, and the number of PRFs processed in this project (all earthquakes were from the Fiji Islands region). Ice core measurements: CCD (Parrenin et al., 2007), BYRD (Bentley, 1972), and NEEM (Montagnat et al., 2014).